Robotics and Computer-Integrated Manufacturing 31 (2015) 21–29

Contents lists available at ScienceDirect

Robotics and Computer-Integrated Manufacturing

journal homepage: www.elsevier.com/locate/rcim

Parameter identification for industrial robots with a fast and robust trajectory design approach

Jingfu Jin, Nicholas Gans *

Department of Electrical Engineering, University of Texas at Dallas, Richardson, TX 75080, USA

ARTICLE INFO

Article history:
Received 26 August 2013
Received in revised form
11 June 2014
Accepted 27 June 2014
Available online 26 July 2014

Keywords:
Identification
Dynamic parameters
Robotics
Trajectory optimization

ABSTRACT

Model-based, torque-level control can offer precision and speed advantages over velocity-level or position-level robot control. However, the dynamic parameters of the robot must be identified accurately. Several steps are involved in dynamic parameter identification, including modeling the system dynamics, joint position/torque data acquisition and filtering, experimental design, dynamic parameters estimation and validation. In this paper, we propose a novel, computationally efficient and intuitive optimality criterion to design the excitation trajectory for the robot to follow. Experiments are carried out for a 6 degree of freedom (DOF) Staubli TX-90 robot. We validate the dynamics parameters using torque prediction accuracy and compare to existing methods. The RMS errors of the prediction were small, and the computation time for the new, optimal objective function is an order of magnitude less than for existing approaches.

1. Introduction

Contemporary applications of robot arms demand high precision and speed, e.g. advanced manufacturing [1] and multi-robot system control [2]. These applications typically require advanced model-based control algorithms or control algorithms based on torque input [3]. Such control schemes require accurate knowledge of the dynamic parameters of robot arm. However, many robot manufacturers do not provide these parameters or provide only partial information [4,5]. Experimental identification or calibration is therefore the only reliable approach to obtain this information.

Many models of robot dynamics have been proposed in the context of dynamic parameter identification. Gautier suggested the energy identification model in [6] and the power model in [7]. The main advantage of these models is that they depend only on functions of joint position and velocity. Researchers have employed inverse dynamic models of robot arms to identify dynamic parameters [5,8–10]. Inverse dynamic models provide more information than the energy or the power model. This additional information allows the creation of well-conditioned over-determined regressor matrices.

There are several ways to estimate the dynamic parameters. Least squares estimation methods [6,11] and maximum likelihood estimation methods [9] are popular approaches. Other approaches include the extended Kalman filter in [12], the total least squares is developed in [13], the online recursive total least squares estimation method in [14], the weighted least squares estimation method [15,16], nonlinear least squares optimization [8], and the instrumental variable approach developed in [17]. Generally, joint angle and torque/current data can be measured directly, but joint velocity and acceleration must be estimated. There are several approaches to estimate velocity and acceleration, including observer/estimators, zero-phase band pass filter, low-pass filters and Kalman filters [6,8,18].

Designing an excitation trajectory is an essential and significant part of improving estimation accuracy. A fifth-order polynomial trajectory in joint space was proposed as an excitation trajectory in [19]. To enable repeatable identification experiments and improve the signal to noise ratio, periodic excitation trajectories based on Fourier series [9], modified Fourier series [5] and finite sum of harmonic sine functions [20] have been proposed. Two optimality criteria have been popular to find optimal periodic trajectories. One is based on minimization of the condition number of the regressor matrix [5,20,21]; another is based on minimization of $\mathbf{log}\{\mathbf{det}(\cdot)\}$ of the Fisher information matrix [20,9]. Since each Fourier series contains $2\times N_i+1$ parameters [22], it can be difficult to solve the optimization problem. Each Fourier series must meet constraints on the trajectory such as initial and final conditions and bounds on position, velocity and acceleration.

Model validation is also an important procedure for confirming the parameter estimation results. Experiment results can directly demonstrate the identification result [9]. Janot et al. discussed the importance of statistical analysis in validating results [17].

* Corresponding author.
E-mail addresses: jingfu.jin@utdallas.edu (J. Jin), ngans@utdallas.edu (N. Gans).

http://dx.doi.org/10.1016/j.rcim.2014.06.004
0736-5845/

A primary contribution of this paper is a novel, simple and intuitive optimal criterion to design the exciting trajectory. Our approach reduces the number of terms that define the trajectory, and we employ Hadamard's inequality, which states that the determinant of a positive definite matrix is less than or equal to the product of its diagonal entries, thus simplifying the optimization problem. For a $m \times n$ rectangular matrix W, the complexity of calculating the upper bound of the determinate using Hadamard's is $O(n)$, but the complexity of calculating the determinate of W^TW is $O(mn^2+n^3)$ and the complexity of calculating the condition number of W is $O(mn^2)$. The use of Hadamard's inequality offers a great reduction in complexity and calculation time in finding the optimal parameters.

We compare our outcome with the two popular optimization functions in terms of computational complexity. Our proposed trajectory performs as well as those found by the existing optimization functions in terms of root mean squared error, and requires an order of magnitude less computation time. We use our algorithm to determine the dynamic parameters of the Staubli TX-90 robot manipulator. To our knowledge, the parameters of this robot have not previously been determined, and this represents a second major contribution of this paper.

The remainder of this paper is organized as follows. Section 2 introduces the background information regarding our experimental dynamic calibration methods. Section 3 describes the proposed excitation trajectory and new optimality criterion. Section 4 provides simulation results that verify the proposed estimation algorithm. Finally, the conclusion is given in Section 5.

2. Background

Our approach employs the inverse dynamic model and the least squares (LS) estimation method to estimate inertia parameters of robot arm. We also use a zero-phase low pass filter to process position data and velocities are calculated with a central difference algorithm. Accelerations are calculated with the central difference algorithm and followed by smoothing, which is performed by the Robust LOcal polynomial regrESSion (RLOESS) smoother [23]. RLOESS has gained widespread acceptance in statistics as an appealing solution for fitting smooth curves to noisy data. The overall procedure of identification is illustrated in Fig. 1

2.1. Dynamic identification model

The dynamic model of an n-link rigid robot can be derived using the Euler–Lagrange or the Newton–Euler formulation [24]. The mathematical model in joint space [25] is given by

$$M(q)\ddot{q}+C(q,\dot{q})\dot{q}+\tau_f=\tau \tag{1}$$

where $q(t)=[q_1(t),\ q_2(t),\ldots,q_n(t)]^T \in \mathbb{R}^n$ is a vector of joint position, and $\dot{q}(t) \in \mathbb{R}^n$ and $\ddot{q}(t) \in \mathbb{R}^n$ are the joint velocity and the acceleration vectors, respectively. $M(q) \in \mathbb{R}^{n\times n}$ is the mass or inertia matrix of the robot, $C(q,\dot{q})$ contains Coriolis, centrifugal and gravitational force terms, $\tau_f(t) \in \mathbb{R}^n$ is the friction forces, and $\tau(t) \in \mathbb{R}^n$ represents the joint torque vector, which is the input to the system. We model the friction forces as

$$\tau_f=f_v\dot{q}+f_c\ \mathrm{sgn}(\dot{q}) \tag{2}$$

where f_v and f_c are constant $n \times n$ diagonal matrices representing viscous and Coulomb friction parameters, respectively, and $\mathrm{sgn}(\cdot)$ is the sign function.

The modified Denavit and Hartenberg (MDH) convention [26] allows us to rewrite the mathematical model (1) in a linearly parametrized form [24] with N_s standard parameters:

$$\tau=Y_s(q,\dot{q},\ddot{q})\beta_s \tag{3}$$

where $Y_s(q,\dot{q},\ddot{q}) \in \mathbb{R}^{n\times N_s}$ is a regressor matrix and $\beta_s \in \mathbb{R}^{N_s\times 1}$ is a vector of standard parameters. For rigid robots, there are 13 standard parameters by each link and joint, including the six components of the inertia matrix of link j at the origin of frame j $(I_{xxj}, I_{xyj}, I_{xzj}, I_{yyj}, I_{yzj}, I_{zzj})$, the first moments of link j (mx_j, my_j, mz_j), the mass (m_j) of link j, the total inertia moment (Ia_j) for rotor and gears of actuator j and viscous and Coulomb friction coefficients (f_{vj}, f_{cj}) [27].

The base parameters are the minimal set of identifiable parameters to parametrize the dynamic equation. They are obtained by regrouping some of the standard parameters by means of linear relations [11,28] or a numerical method with respect to the QR decomposition [29]. Then the dynamics equation with N_b identifiable base parameters can be addressed as

$$\tau=Y(q,\dot{q},\ddot{q})\beta \tag{4}$$

where $\beta \in \mathbb{R}^{N_b}$ are the base parameters and $Y(q,\dot{q},\ddot{q}) \in \mathbb{R}^{n\times N_b}$ is a subset of the independent columns of Y_s [30].

An excitation reference trajectory must be used to persistently excite the given system. In this work, we employ a periodic trajectory. Assume that the joint positions and motor torques are measured at a sampling frequency of ω_s, and denote the kth sampling time as t_k. If the fundamental frequency of the trajectories is w_f, we can collect $M=\omega_s/w_f$ samples over one period T. These measurements can be used to obtain an over-determined set of equations [31]:

$$\mathbf{\Gamma}=W\beta+\rho \tag{5}$$

where

$$W=\begin{bmatrix} Y(q(t_1),\dot{q}(t_1),\ddot{q}(t_1))_{n\times N_b} \\ Y(q(t_2),\dot{q}(t_2),\ddot{q}(t_2))_{n\times N_b} \\ \vdots \\ Y(q(t_M),\dot{q}(t_M),\ddot{q}(t_M))_{n\times N_b} \end{bmatrix}$$

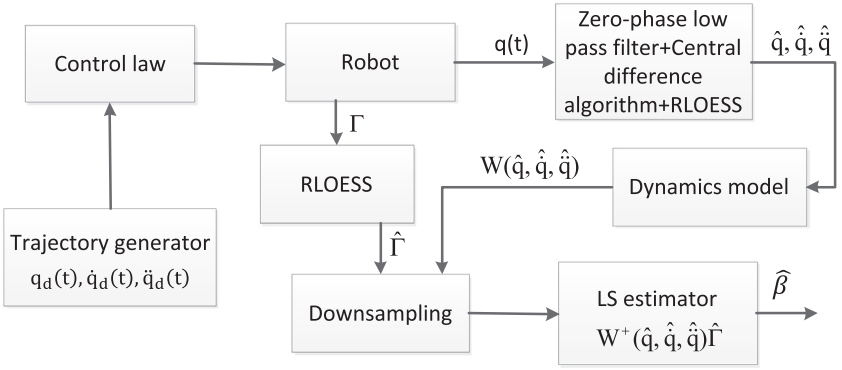

Fig. 1. The proposed parameter identification process.

is the observation matrix, $\mathbf{\Gamma} = [\tau(t_1)^T \tau(t_2)^T \ldots \tau(t_M)^T]^T \in \mathbb{R}^{nM}$ and $\rho \in \mathbb{R}^{nM}$ is the vector of errors due to complex friction, modeling error, measurement noise, etc. Therefore, measurement of torque/force may differ from the actual motor torques. The dimension of the observation matrix W depends on the number of samples collected and is $nM \times N_b$.

2.2. Least squares parameter estimator

We employ the LS estimator to solve the over-determined set of equations. The matrix notation is given by

$$\hat{\beta} = \min_{\beta} \|\mathbf{\Gamma} - \mathrm{W}\beta\|^2 = \mathrm{W}^{+}\mathbf{\Gamma} \tag{6}$$

where $\mathrm{W}^{+} = (\mathrm{W}^T\mathrm{W})^{-1}\mathrm{W}^T$ and $\hat{\beta} \in \mathbb{R}^{N_b}$ is the estimated base parameters. The covariance matrix of the estimation error of $\hat{\beta}$ is $\sigma^2 I$, where $\sigma^2 \in \mathbb{R}$ is the variance of the errors. As σ^2 is generally unknown, we take an estimate of σ^2 as [31]

$$\hat{\sigma}^2 = \frac{1}{nM - N_b} \| \mathbf{\Gamma} - \mathrm{W}\hat{\beta} \|^2. \tag{7}$$

The covariance matrix of the estimation error is given by

$$\sigma_{ls} = \mathrm{E}[(\beta - \hat{\beta})(\beta - \hat{\beta})^T] = \hat{\sigma}^2 (\mathrm{W}^T\mathrm{W})^{-1} \tag{8}$$

and $\sigma_{ls}(j,j)$ is the j$^{\text{th}}$ element of σ_{ls}. The relative standard deviation (RSD) of the j$^{\text{th}}$ parameter is

$$\%\sigma_{\hat{\beta}_j} = 100 \frac{\sqrt{\sigma_{ls}(j,j)}}{|\hat{\beta}_j|}. \tag{9}$$

We calculated the dynamic parameters using weighted least squares (WLS) [15,16] and total least squares (TLS) [13] in addition to LS. However, in our case the identification result did not significantly improve over LS. Therefore, we employ LS since LS is simpler.

2.3. Signal processing

The collected data (e.g., position and torque data) may be affected by some error or noise. Decreasing the effects of noise on W and $\mathbf{\Gamma}$ is an essential step to improve the accuracy of the parameter estimation result. Positions are calculated by means of a zero-phase low-pass filter (forward and reverse IIR Butterworth filters). Velocities are calculated with a central difference algorithm. Accelerations are calculated with the central difference algorithm and followed by smoothing, which is performed by RLOESS, implemented using the MATLAB `smooth` function. RLOESS is a regression method that employs a moving average filter and performs residual analysis to remove outliers before smoothing [23]. We also employ RLOESS to remove noise and torque ripples of the collected torque data. To remove information-free samples, a down-sampling is conducted on W and $\mathbf{\Gamma}$ using a decimate filter [7].

3. Experimental design

Experiment design usually consists of two steps. The first step is trajectory parameter selection and the second step is parameter optimization. We propose a novel, modified Fourier series, which can generate a persistent excitation trajectory at a greatly reduced level of complexity and computation time necessary for the optimization process.

3.1. Trajectory parametrization

The trajectory for each joint is a finite sum of N harmonic sine and cosine functions. The joint position q_i, velocity $\dot{q}_i$, and acceleration $\ddot{q}_i$ trajectories for the ith joint of an n-link robot are given as

$$q_i(t) = \sum_{l=1}^{N} \frac{a_l}{\omega_f l} \sin(\omega_f l t) - \frac{b_l}{\omega_f l} \cos(\omega_f l t) + q_{i0} \tag{10}$$

$$\dot{q}_i(t) = \sum_{l=1}^{N} a_l \cos(\omega_f l t) + b_l \sin(\omega_f l t) \tag{11}$$

$$\ddot{q}_i(t) = \omega_f \sum_{l=1}^{N} b_l l \cos(\omega_f l t) - a_l l \sin(\omega_f l t) \tag{12}$$

where ω_f is the fundamental frequency and $q_{i\,0}$ is the offset of the joint position of the excitation reference trajectories [32]. All joints share the same fundamental frequency to guarantee the periodicity of the trajectory [9]. Hence, each trajectory contains only $2N+1$ *parameters*, which generate the excitation reference trajectory. The parameters a_l and b_l determine the amplitudes of the cosine and sine functions and can be determined through optimization or with trial and error. The trade-off of choosing fundamental frequency was discussed in Swevers's work [32].

3.2. Trajectory optimization

The problem of determining an excitation trajectory $\mathbf{q}^*(t)$ can be formulated as

$$\mathbf{q}^*(t) = \mathrm{argmin}(\mathbf{J}) \tag{13}$$

subject to

$$\begin{cases} |q_i(t)| \le q_{max} & \forall i,t \text{ (a)} \\ |\dot{q}_i(t)| \le v_{max} & \forall i,t \text{ (b)} \\ |\ddot{q}_i(t)| \le a_{max} & \forall i,t \text{ (c)} \\ q_i(t_0) = q_i(t_f) = 0 & \forall i,t \text{ (d)} \\ \dot{q}_i(t_0) = \dot{q}_i(t_f) = 0 & \forall i,t \text{ (e)} \\ \ddot{q}_i(t_0) = \ddot{q}_i(t_f) = 0 & \forall i,t \text{ (f)} \end{cases} \tag{14}$$

where $\mathbf{J}$ is an objective function to be determined subsequently, and q_{max} (rad), v_{max} (rad s^{-1}) and a_{max}(rad s^{-2}) denote bounds on joint position, velocity and acceleration, respectively. Unexpected behavior will result at the start and end points if $\dot{q}_i(t_0) \neq 0$, $\dot{q}_i(t_f) \neq 0$, $\ddot{q}_i(t_0) \neq 0$ and $\ddot{q}_i(t_f) \neq 0$ [5]. Therefore constraints (14e) and (14f) are added to remedy this defect.

Substituting (10a) into (14a), we have

$$\begin{aligned} |q_i(t)| &= \left| \sum_{l=1}^{N} \frac{a_l}{\omega_f l} \sin(\omega_f l t) - \frac{b_l}{\omega_f l} \cos(\omega_f l t) + q_{i0} \right| \\ &\le \sum_{l=1}^{N} \frac{1}{l\omega_f} \sqrt{(a_l^2 + b_l^2)} + |q_{i0}| \le q_{max}. \end{aligned} \tag{15}$$

Similarly,

$$\begin{aligned} |\dot{q}_i(t)| &= \left| \sum_{l=1}^{N} a_l \cos(\omega_f l t) + b_l \sin(\omega_f l t) \right| \\ &\le \sum_{l=1}^{N} \sqrt{(a_l^2 + b_l^2)} \le v_{max} \end{aligned} \tag{16}$$

$$\begin{aligned} |\ddot{q}_i(t)| &= \omega_f \left| \sum_{l=1}^{N} -a_l l \sin(\omega_f l t) + b_l l \cos(\omega_f l t) \right| \\ &\le \omega_f \sum_{l=1}^{N} l \sqrt{(a_l^2 + b_l^2)} \le a_{max}. \end{aligned} \tag{17}$$

In addition, the constraint (14d)–(14f) can be rewritten as

$$q_i(t_0) = q_i(0) = \sum_{l=1}^{N} \frac{b_l}{\omega_f l} + q_{i0} = 0 \tag{18}$$

$$\dot{q}_i(t_0) = \dot{q}_i(0) = \sum_{l=1}^{N} a_l = 0 \tag{19}$$

$$\ddot{q}_i(t_0) = \ddot{q}_i(0) = \sum_{l=1}^{N} \omega_f l b_l = 0. \tag{20}$$

In the literature, there are several ways to find optimal excitation trajectories. In particular, the excitation trajectory was optimized by minimizing the condition number of the observation matrix W [5,20,21] or $\mathbf{log}\{\mathbf{det}(W^T W)\}$ [9,20].

3.3. Proposed objective function using Hadamard's inequality

According to Hadamard's inequality, the determinant of a positive definite matrix is less than or equal to the product of its diagonal entries [33]. For a $m \times n$ rectangular matrix W, the complexity of calculating the upper bound of the determinate using Hadamard's is $O(n)$, but the complexity of calculating the determinate of $W^T W$ is $O(mn^2 + n^3)$ and the complexity of calculating the condition number of W is $O(mn^2)$. To estimate dynamic parameters, we usually collect more than thousand samples. In our case, the size of the observation matrix W is 11250×52. Clearly, applying Hadamard's inequality reduces in complexity and calculation time finding the optimal parameters. A comparison of execution times is given in Section 4.5.

In applying Hadamard's inequality, we have

$$\begin{aligned} \mathbf{det}(W^T W) &\le \sum_{k=1}^{nM} W_{k1}^2 \sum_{k=1}^{nM} W_{k2}^2 \cdots \sum_{k=1}^{nM} W_{kN_b}^2 \\ &\le \prod_{g=1}^{N_b} \sum_{k=1}^{nM} W_{kg}^2. \end{aligned} \tag{21}$$

where W_{kg} is the kth element of the gth column of the regressor matrix W. We define the summation of W_{kg}^2 as W_g^s, and rewrite (21) as

$$\mathbf{det}(W^T W) \le \prod_{g=1}^{N_b} W_g^s. \tag{22}$$

Therefore, maximizing $\prod_{g=1}^{N_b} W_g^s$, subject to the constraints, will maximize the upper bound of $\mathbf{det}(W^T W)$ and ideally make the determinate larger. Our experimental results demonstrate that our method works as well as other methods (i.e., directly optimizing the condition number or log determinate) in terms of root-mean-square (RMS) error of the torque prediction and greatly reduces complexity and calculation time needed to find the optimal parameters. Therefore, we take the objective function as

$$\mathbf{J}_1 = \frac{1}{\prod_{g=1}^{N_b} W_g^s} \tag{23}$$

subject to

$$\begin{cases} |q_i(t)| \le q_{max} & \forall i,t \text{ (a)} \\ |\dot{q}_i(t)| \le v_{max} & \forall i,t \text{ (b)} \\ |\ddot{q}_i(t)| \le a_{max} & \forall i,t \text{ (c)} \\ q_i(t_0) = q_i(t_f) = 0 & \forall i,t \text{ (d)} \\ \dot{q}_i(t_0) = \dot{q}_i(t_f) = 0 & \forall i,t \text{ (e)} \\ \ddot{q}_i(t_0) = \ddot{q}_i(t_f) = 0 & \forall i,t \text{ (f)} \end{cases} \tag{24}$$

In our experiment, the persistent excitation trajectories were designed with $a_l \neq 0$, $b_l \neq 0$ and $N=5$. The optimization problem can be solved by any appropriate means, such as `family fmincon` in the MATLAB Optimization toolbox with the predetermined offsets $q_{i\ 0}$. The physical limitation on joint positions, velocities

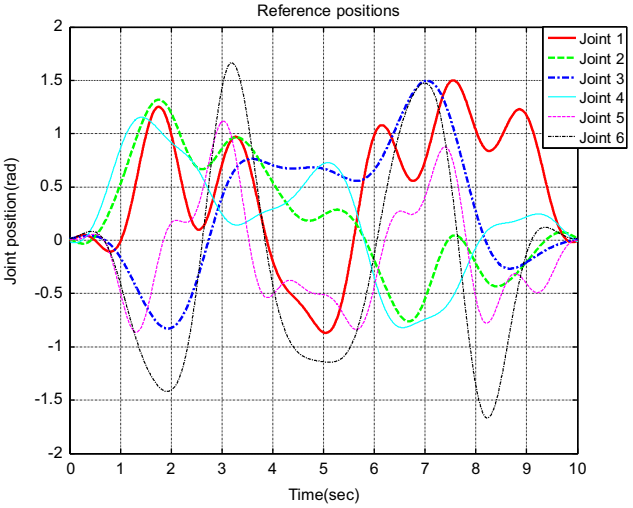

Fig. 2. Reference trajectory.

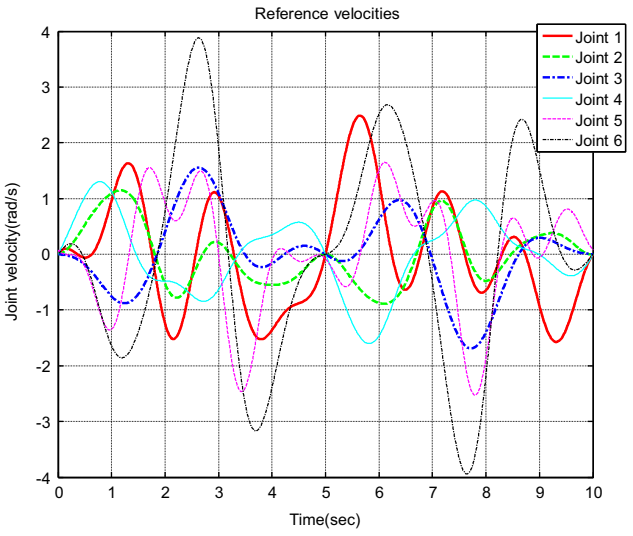

Fig. 3. Reference velocity.

Table 1
The range, speed and resolution.

Axis	1	2	3	4	5	6
Range (deg)	360	277.5	280	540	255	540
Working range dist. (deg)	±180	−130 +147.5	±140	±270	−115 +140	±270
Nominal speed (deg/s)	250	200	300	430	350	600
Ang. resolution (deg 10^{-3})	0.057	0.057	0.057	0.057	0.122	0.183

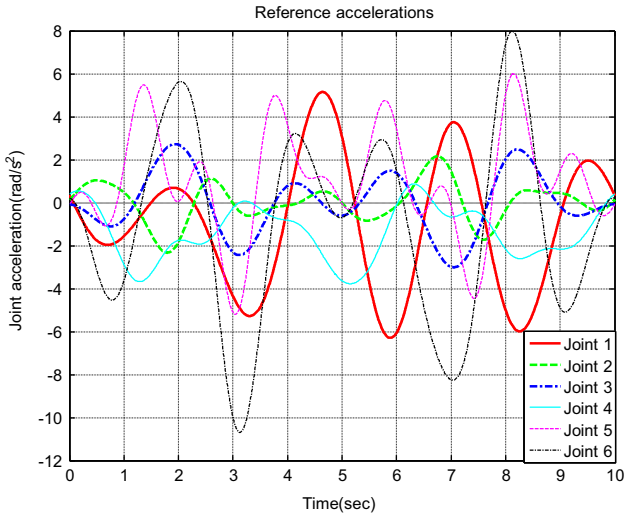

Fig. 4. Reference acceleration.

and accelerations of the Staubli TX-90 robot is given in Table 1 [34].

The initial conditions used for optimization are randomly generated for each link. Then, we can generate the reference excitation trajectories with optimal parameters. An example of typical joint position, velocity and acceleration trajectories is shown in Figs. 2–4. Note that the start and end points of reference velocity and acceleration are zero or close to zero in Figs. 3 and 4. This result satisfies constraints (14e) and (14f).

4. Experiment and validation

To verify the proposed estimation algorithm and trajectory, the dynamic parameters of the Staubli TX-90 robot were identified.

4.1. Experimental testbed

The Staubli TX-90 robot has a serial structure with six rotational joints, as seen in Fig. 5. The link frames of the Staubli TX-90 robot are illustrated in Fig. 6 and its MDH parameters are given in Table 2.

We define the position variable of joint i as θ_i. Moreover, the variables of joints 2 and 3 in the present relationship are acquired from the measured values of joints 2 and 3 using the relations, $\theta_2 = \theta_{2staubli} - \pi/2$ and $\theta_3 = \theta_{3staubli} + \pi/2$ [13]. Some robots, such as the Staubli TX-40 [30] and Staubli RX-90 [27], have a coupling effect between the two last wrist joints. However, the two last wrist joints are not coupled in the TX-90.

We employed the software SYMORO+ to compute the customized symbolic expressions of the models [26]. For the TX-90 robot, a subset of the standard parameters discussed in Section 1 can be regrouped to generate a reduced set of base parameters as

$$
\begin{aligned}
I_{zz_1r} &= (m_3+m_4+m_5+m_6)(d_2^2+d_3^2+r_3^2) \\
&\quad + Ia_1 + d_2^2 m_2 + 2mz_3 r_3 + I_{yy_2} + I_{yy_3} + I_{zz_1} \\
I_{xx_2r} &= -(m_3+m_4+m_5+m_6)(d_3^2+r_2^2-r_3^2) \\
&\quad + I_{xx_2} - I_{yy_2} \\
I_{xz_2r} &= xz_2 - d_3(m_3+m_4+m_5+m_6+mz_3)r_3 \\
I_{zz_2r} &= Ia_2 + d_3^2(m_3+m_4+m_5+m_6) + I_{zz_2} \\
mx_{2r} &= d_3(m_3+m_4+m_5+m_6) + mx_2 \\
I_{xx_3r} &= 2mz_4 r_4 + (m_4+m_5+m_6)r_4^2 \\
&\quad + I_{xx_3} - I_{yy_3} + I_{yy_4}
\end{aligned}
$$

Fig. 5. Staubli TX-90 robot.

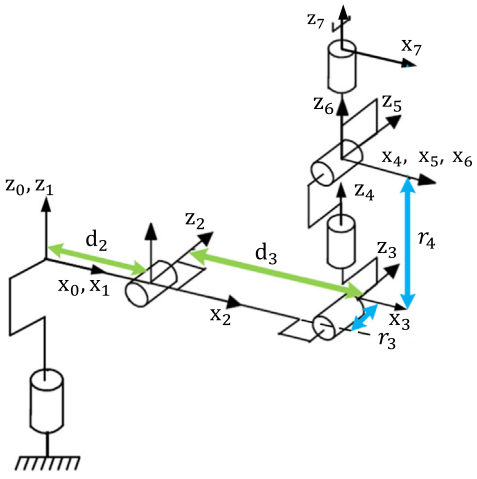

Fig. 6. Link frame of Staubli TX-90 robot.

Table 2
The MDH parameter.

Link	r_i (mm)	α_i	d_i (mm)	θ_i
1	0	0	0	θ_1
2	0	$-\pi/2$	50	$\theta_2 - \pi/2$
3	50	0	425	$\theta_3 + \pi/2$
4	425	$\pi/2$	0	θ_4
5	0	$-\pi/2$	0	θ_5
6	0	$\pi/2$	0	θ_6

$$
\begin{aligned}
I_{zz_3r} &= 2mz_4 r_4 + (m_4+m_5+m_6)r_4^2 + I_{yy_4} + I_{zz_3} \\
my_{3r} &= my_3 - mz_4 - (m_4+m_5+m_6)r_4 \\
I_{xx_4r} &= I_{xx_4} - I_{yy_4} + I_{yy_5} \\
I_{zz_4r} &= I_{yy_5} + I_{zz_4} \\
my_{4r} &= I_{my_4} + I_{mz_5} \\
I_{xx_5r} &= I_{xx_5} - I_{yy_5} + I_{yy_6} \\
I_{zz_5r} &= I_{yy_6} + I_{zz_5} \\
my_{5r} &= I_{my_5} - I_{mz_6} \\
I_{xx_6r} &= I_{xx_6} - I_{yy_6}.
\end{aligned}
$$

Table 3
The base parameters.

Link 1	Link 2	Link 3	Link 4	Link 5	Link 6
0	I_{xx_2r}	I_{xx_3r}	I_{xx_4r}	I_{xx_5r}	I_{xx_6r}
0	I_{xy_2}	I_{xy_3}	I_{xy_4}	I_{xy_5}	I_{xy_6}
0	I_{xz_2r}	I_{xz_3}	I_{xz_4}	I_{xz_5}	I_{xz_6}
0	I_{yz_2}	I_{yz_3}	I_{yz_4}	I_{yz_5}	I_{yz_6}
I_{zz_1r}	I_{zz_2r}	I_{zz_3r}	I_{zz_4r}	I_{zz_5r}	I_{zz_6}
0	mx_{2r}	mx_3	mx_4	mx_5	mx_6
0	my_2	my_{3r}	my_{4r}	my_{5r}	my_6
0	0	Ia_3	Ia_4	Ia_5	Ia_6
f_{v1}	f_{v2}	f_{v3}	f_{v4}	f_{v5}	f_{v6}
f_{c1}	f_{c2}	f_{c3}	f_{c4}	f_{c5}	f_{c6}

The remaining standard parameters cannot be regrouped and are considered base parameters. The base parameters associated with each link are given in Table 3.

4.2. Data acquisition and filtering

We choose the fundamental frequency of the trajectories as 0.1 Hz; this gives excitation trajectories with a period of 10 s. The robot control system can collect the joint positions and torques (which are sampled synchronously at a frequency of 62.5 Hz) while the robot tracks the reference trajectory. Noting the start and end positions, velocities and accelerations are the same, we repeated the persistent excitation trajectories three times. Therefore we have 625 samples available for estimating the dynamic parameters.

As described in Section 2.3, the joint position $\hat{q}$ was processed using a 0.5 Hz cut-off frequency low-pass, zero-phase filter, and the joint velocity $\dot{\hat{q}}$ was calculated by using a central difference algorithm of $\hat{q}$. Moreover, the acceleration $\ddot{\hat{q}}$ was calculated by using a central difference algorithm of $\dot{\hat{q}}$ and was then processed using RLOESS with a span of 2.0%. Torque measurements were also processed with RLOESS with a span of 1.5% to remove noise. For comparison purposes, we also used a traditional low-pass filter to remove the torque noise. The low pass filter (FIR equiripple filter) was created with a passband frequency of 0.016 rad/sample, a stopband frequency of 0.16 rad/sample (0.5 rad/sample), a passband ripple of 1 dB, and a stopband attenuation of 3 dB. Finally, we downsample for W and $\boldsymbol{\Gamma}$ by a factor of 2 using a decimate filter. Comparing the results of using RLOESS and the traditional low-pass filter, the RLOESS was found to perform better in terms of RMS errors.

4.3. Parameter estimation

We constructed the observation matrix W with the measured joint position and estimated velocity and acceleration samples. The condition number of the observation matrix for all the samples was 108, indicating that the system is well excited.

The standard LS estimation method was used to get the dynamics parameters of the Staubli TX-90 robot. Some dynamic parameters with a small magnitude have no significant contribution to generating the torque, so they remain poorly identifiable and can be removed in order to simplify the dynamics model [27]. After discarding the dynamic parameters with a large RSD (RSD > 20%) calculated from Eq. (9), 29 essential parameters which are used to describe the dynamics model of the Staubli TX-90 robot are obtained. The dynamic parameters are given in Table 4.

Table 4
The estimated dynamic parameters.

Parameters	$\hat{\beta}$	rsd (%)	σ_β
I_{zz_1r} (kg m^2)	19.44	2.25	0.43
f_{v1} (N m/rad s^{-1})	68.96	0.60	0.41
f_{c1} (N m/rad s^{-1})	21.37	1.51	0.32
I_{xx_2r} (kg m^2)	−9.88	4.28	0.42
I_{xy_2r} (kg m^2)	−5.68	3.45	0.19
I_{xz_2r} (kg m^2)	−1.10	16.75	0.18
I_{zz_2r} (kg m^2)	12.24	2.71	0.33
mx_{2r} (kg m)	−14.28	0.38	0.05
f_{v2} (N m/rad s^{-1})	72.68	1.03	0.75
f_{c2} (N m/rad s^{-1})	21.27	1.76	0.37
I_{xz_3} (kg m^2)	−1.17	10.68	0.12
I_{zz_3r} (kg m^2)	4.14	4.19	0.17
mx_3 (kg m)	−0.39	15.17	0.06
my_{3r} (kg m)	4.07	1.31	0.05
Ia_3 (kg m^2)	−1.88	6.46	0.12
f_{v3} (N m/rad s^{-1})	15.27	2.29	0.34
f_{c3} (N m/rad s^{-1})	5.80	5.21	0.30
I_{xz_4} (kg m^2)	0.48	13.02	0.06
I_{zz_4r} (kg m^2)	−0.70	15.33	0.10
mx_4 (kg m)	0.48	13.66	0.06
my_{4r} (kg m)	−0.18	18.63	0.03
f_{v4} (N m/rad s^{-1})	10.00	3.03	0.30
f_{c4} (N m/rad s^{-1})	4.70	6.29	0.29
I_{xx_4r} (kg m^2)	0.77	13.03	0.10
I_{yz_5} (kg m^2)	−0.32	17.05	0.05
f_{v5} (N m/rad s^{-1})	6.77	4.59	0.31
f_{c5} (N m/rad s^{-1})	4.71	6.29	0.29
f_{v6} (N m/rad s^{-1})	3.37	3.86	0.13
f_{c6} (N m/rad s^{-1})	5.05	5.33	0.26

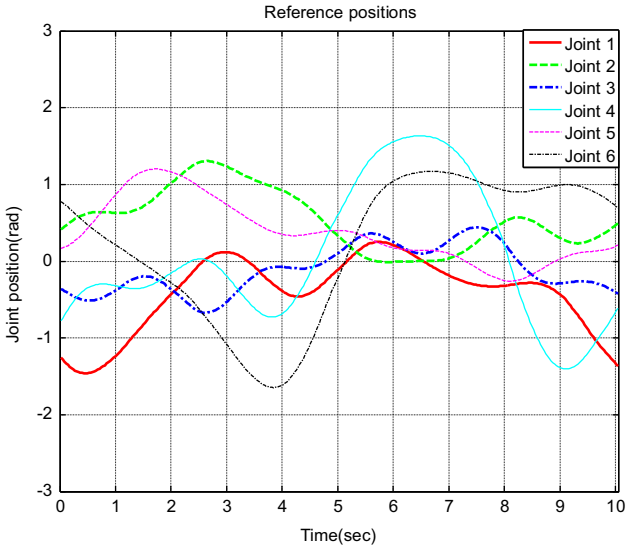

Fig. 7. Validation trajectories.

4.4. Validation

Model validation is an essential procedure before we apply the dynamics parameters in control applications. The validation is carried out by comparing the measured torque Γ and the estimated torque $W\hat{\beta}$. A new validation trajectory was generated, as shown in Fig. 7. The estimated and measured torques running the persistent excitation trajectory and validation trajectory are shown in Figs. 8 and 9, respectively. The green-dash-dot lines in Figs. 8 and 9 are the prediction error, which is notably small.

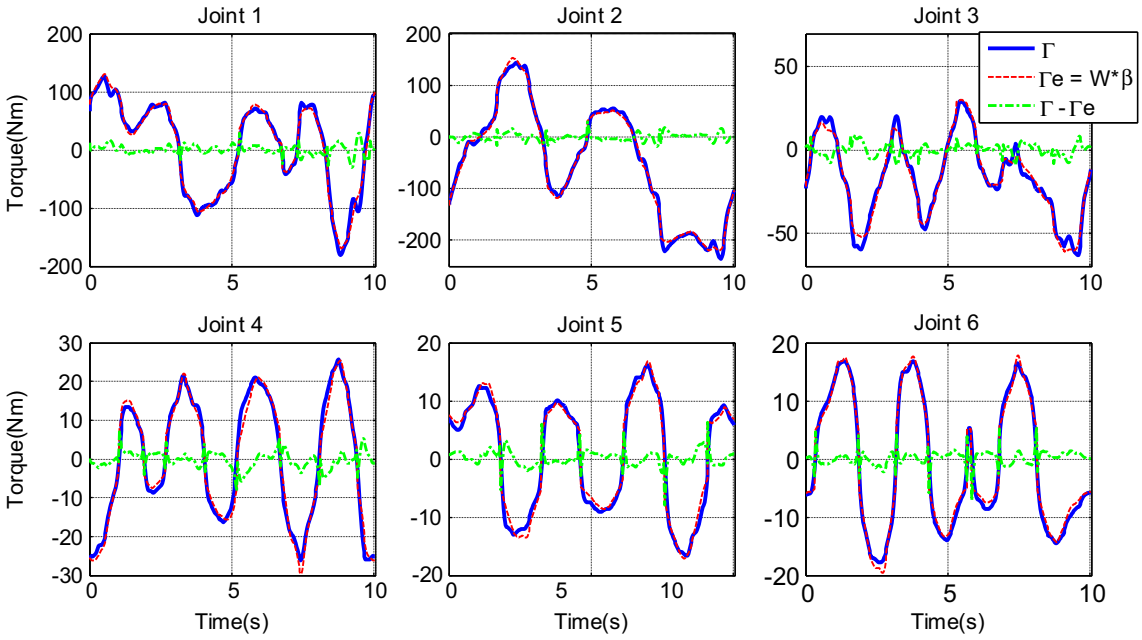

Fig. 8. The comparison of the measured and the predicted torque with the given excitation trajectory. The blue-solid lines are the measured torques, the red-dashed lines are the predicted torques, and green-dash-dot lines are the torque errors. (For interpretation of the references to color in this figure caption, the reader is referred to the web version of this paper.)

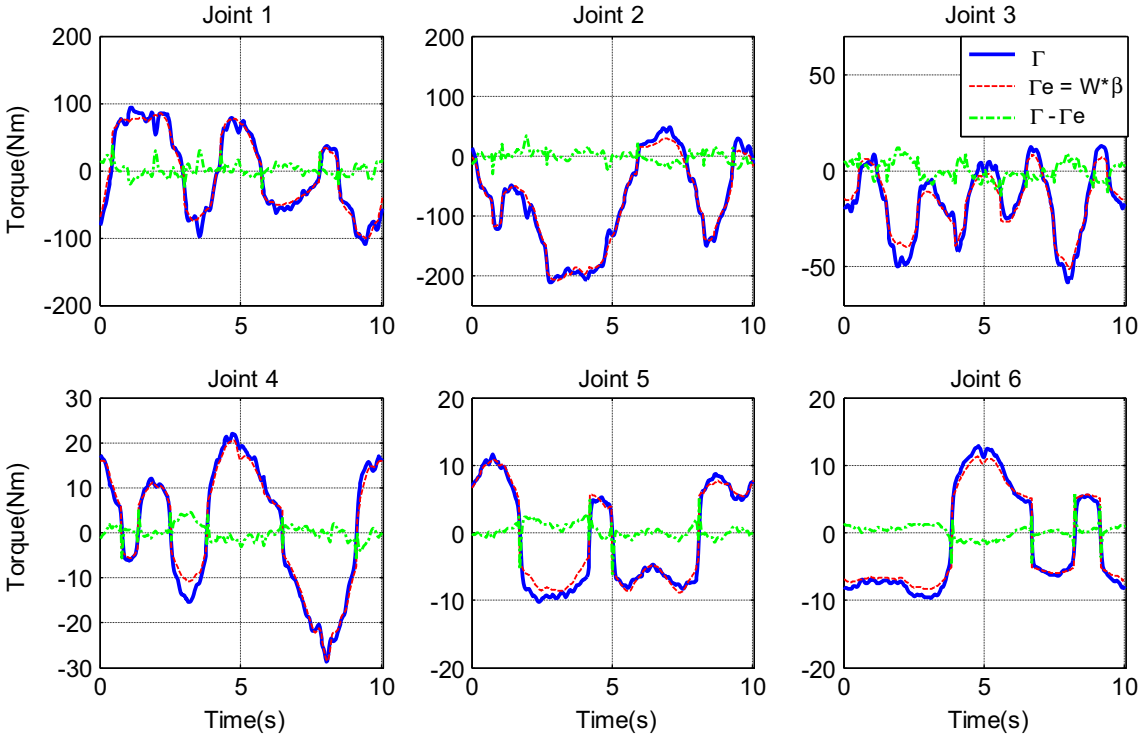

Fig. 9. The comparison of the measured and the predicted torque with a validation trajectory. The blue-solid lines are the measured torques, the red-dashed lines are the predicted torques, and green-dash-dot lines are the torque errors. (For interpretation of the references to color in this figure caption, the reader is referred to the web version of this paper.)

However, we can see a spike when the velocity crosses zero, due to the friction forces at low velocities. We also compared the RMS errors between the predicted torques and the averaged measured torques from tracking a set of excitation and validation trajectories in Table 5. These errors are similar in magnitude to other researchers' recent work in [5,32]. Therefore, the identified dynamic parameters are confirmed to work under multiple trajectories.

We also estimated the torque measurement with a well-tuned low pass filter, and then we estimated the dynamic parameters using the same joint positions, velocities and accelerations of the persistent excitation trajectories. The torque prediction results are given in Fig. 10. The RMS errors of the predicted torques of RLOESS and a well-tuned low pass filter are compared in Table 6.

4.5. Comparison of the proposed optimization to common objective functions

We have compared the computing time and the RMS error of predicted torques from our optimizing our proposed objective function in (23) with respect to two popular objective functions. The first is

$$\mathbf{J}_2 = \mathbf{log}\{\mathbf{det}(\mathrm{W}^T\mathrm{W})\} \tag{25}$$

which is the observation matrix related to the LS estimator [9,20]. The second objective function is

$$\mathbf{J}_3 = \mathrm{cond}(\mathrm{W}) \tag{26}$$

which is based on the condition number of the observation matrix [5,20]. We have used the `fmincon` solver in MATLAB to minimize the objective function $\mathbf{J}_2$ in (25) and $\mathbf{J}_3$ in (26). The starting points for the optimization are randomly selected for both $\mathbf{J}_2$ and $\mathbf{J}_3$. The specifications of the PC we used include an Intel Core i7 (SMP), 8 GB of RAM, and 64-bit Operating system. Here we used 625 samples to build an observation matrix $\mathrm{W} \in \mathbb{R}^{3750\times 52}$.

The comparison of execution times is given in Table 7, which shows that the CPU time of execution for the proposed objective function is much faster than the cond(W) based or det ($\mathrm{W}^T\mathrm{W}$) based objective functions. Average execution time for the proposed objective function is approximately $\frac{1}{16}$ of the $\mathbf{J}_2$ and $\frac{1}{19}$ of $\mathbf{J}_3$. A comparison of torque prediction RMS errors over the resulting excitation trajectories for all the three objective functions is given in Table 8. Our analysis found that the RMS error of $\mathbf{J}_1$ is smaller than or close to the others.

Table 5
RMS errors of the torque prediction for both tracking the excitation and the validation trajectories.

Joint #	Excitation traj. (N m)	Validation traj. (N m)
Joint 1	8.76	10.79
Joint 2	7.35	10.60
Joint 3	3.62	4.83
Joint 4	2.20	1.83
Joint 5	1.44	1.22
Joint 6	1.32	1.06
Sum	24.71	30.37

5. Conclusion

In this paper, Hadamard's inequality is used to propose a novel, simple and intuitive criterion for optimizing an excitation

Table 6
A comparison of RMS of the torque prediction error using RLOESS and low pass filter.

Joint #	RLOESS (RMS error) (N m)	Low pass filter (RMS error) (N m)
Joint 1	8.76	9.22
Joint 2	7.35	9.20
Joint 3	3.62	3.69
Joint 4	2.20	2.97
Joint 5	1.44	2.00
Joint 6	1.32	2.23
Sum	24.71	29.32

Table 7
A comparison of execution time.

Joint #	$\mathbf{J}_1$	$\mathbf{J}_2$	$\mathbf{J}_3$
Exe. time	36 s	≈ 586 s	≈ 673 s
Ave. exe. time (100 times)	35 s	–	–

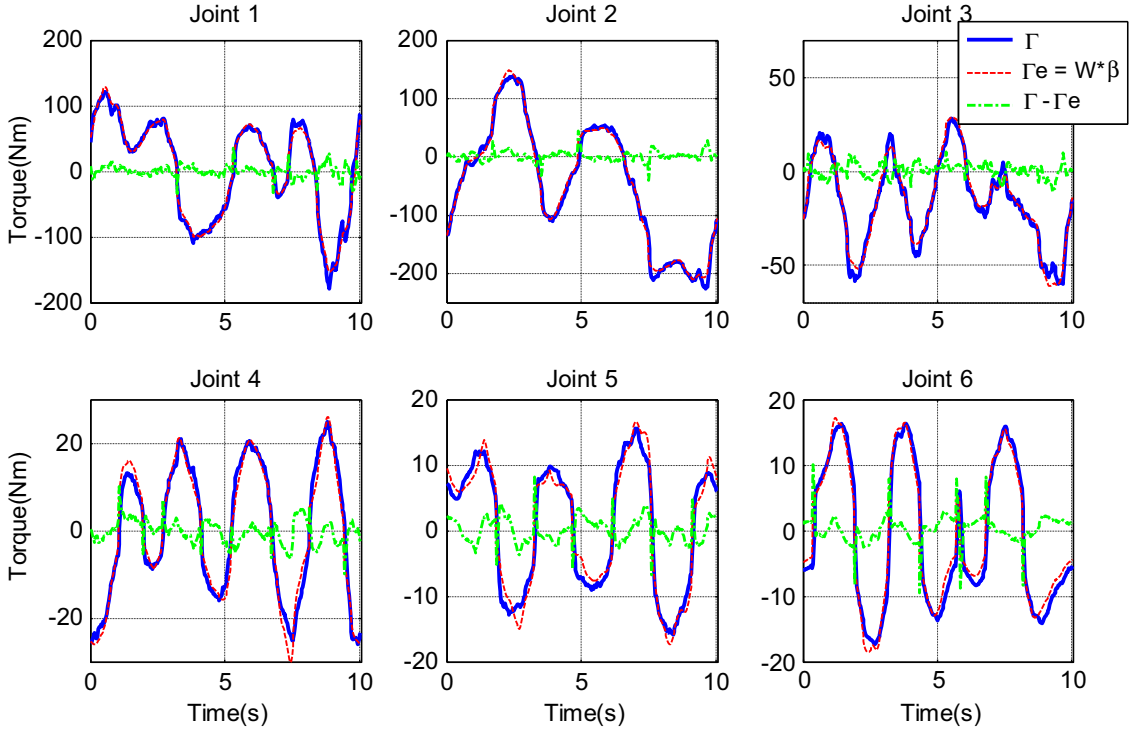

Fig. 10. The comparison of the measured and the predicted torque with the given excitation trajectory using a low pass filter. The blue-solid lines are the measured torques, the red-dashed lines are the predicted torques, and green-dash-dot lines are the torque errors. (For interpretation of the references to color in this figure caption, the reader is referred to the web version of this paper.)

Table 8
RMS errors of the torque prediction for $\mathbf{J}_1$, $\mathbf{J}_2$ and $\mathbf{J}_3$.

Joint #	$\mathbf{J}_1$ (N m)	$\mathbf{J}_2$ (N m)	$\mathbf{J}_3$ (N m)
Joint 1	8.76	5.88	8.11
Joint 2	7.35	9.36	7.66
Joint 3	3.62	3.26	5.83
Joint 4	2.20	1.87	2.57
Joint 5	1.44	2.24	3.09
Joint 6	1.32	1.11	1.18
Sum	24.7	23.7	28.46

trajectory used for dynamic parameter identification. The proposed excitation trajectories also are zero or close to zero at the start and end points. The dynamic parameters of a 6 DOF Staubli TX-90 robot were accurately identified with respect to the proposed excitation trajectory. After discarding the dynamic parameters with a large RSD, we keep 29 essential dynamic parameters to describe the dynamic model of the Staubli TX-90 robot. To validate the reliability of the dynamic parameters, we ran the robot with new trajectories, which were not used in the parameter estimation, and compared the measured and the predicted torques. RMS errors were small, with magnitude similar to those reported by other recent researchers. The execution time and accuracy of the each optimization was compared to popular existing methods. The computation time for the proposed objective function is an order of magnitude less than the two popular objective functions while returning accurate estimated parameters.

Acknowledgments

The authors would like to thank Wisama Khalil at IRCCyN for helping us with the software SYMORO+ to automatically compute the customized symbolic expressions of the dynamic model of the Staubli TX-90 robot. Thanks also to the anonymous reviewers for valuable suggestions that improved the proposed methodology, results, and paper.

This work was supported in part by DGIST R&D Program of the Ministry of Education, Science and Technology of Korea (14-BD-01).

References

[1] Roy B, Asada H. Nonlinear feedback control of a gravity-assisted underactuated manipulator with application to aircraft assembly. IEEE Trans Robot 2009;25:1125–33.
[2] Brogrdh T. Robot control overview: an industrial perspective. Model Identif Control 2009;30:167–80.
[3] Wu J, Wang J, You Z. An overview of dynamic parameter identification of robots. Robot Comput Integr Manuf 2010;26:414–9.
[4] Ayusawa K, Venture G, Nakamura Y. Identification of humanoid robots dynamics using floating-base motion dynamics. In: Proceedings of IEEE/RSJ international conference on intelligent robots and systems, 2009, p. 2854–9.
[5] Wu W, Zhu S, Wang X, Liu H. Closed-loop dynamic parameter identification of robot manipulators using modified fourier series, Int J Adv Robots Syst (2012), 9, http://dx.doi.org/10.5772/45818.
[6] Gautier M, Khalil W, Restrepo P. Identification of the dynamic parameters of a close loop robot. In: International conference on robotics and automation. p. 3045–50.
[7] Gautier M. Dynamic identification of robots with power model. In: International conference on robotics and automation, 1997, p. 1922–27.
[8] Gautier M, Janot A, Vandanjon P-O. A new closed-loop output error method for parameter identification of robot dynamics. IEEE Trans Control Syst Technol 2013;21:428–44.
[9] Swevers J, Ganseman C, Tukel DB, Joris De Schutter aHVB. Optimal robot excitation and identification. IEEE Trans Robot Autom 1997;13:730–40.
[10] Kostic D, de Jager B, Steinbuch M, Hensen R. Modeling and identification for high-performance robot control: an RRR-robotic arm case study. IEEE Trans Control Syst Technol 2004;18:55–68.
[11] Gautier M, Khalil W. Direct calculation of minimum set of inertial parameters of serial robots. IEEE Trans Robot Autom 1990;6:368–73.
[12] Gautier M, Poignet P. Extended Kalman filtering and weighted least squares dynamic identification of robot. Control Eng Pract 2001;9:1361–72.
[13] Briot S, Gautier M. Global identification of joint drive gains and dynamic parameters of parallel robots. Multibody Syst Dyn 2013:1–24.
[14] Kubus D, Krger T, Wahl FM. On-line estimation of inertial parameters using a recursive total least-squares approach. In: International conference on robotics and automation, 2008, p. 3845–52.
[15] Poignet P, Gautier M. Comparison of weighted least squares and extended Kalman filtering methods for dynamic identification of robots. In: International conference on robotics and automation, 2000, p. 3622–27.
[16] Zak G, Benhabib B, Fenton RG, Saban I. Application of the weighted least squares parameter estimation method to the robot calibration. IEEE/ASME J Mech Des 1994;116:890–3.
[17] Janot A, Vandanjon P, Gautier M. A generic instrumental variable approach for industrial robot identification. IEEE Trans Control Syst Technol 2014;22:132–45.
[18] Han J, He Y, Xu W. Angular acceleration estimation and feedback control: an experimental investigation. Mechatronics 2007:524–32.
[19] Atkeson CG, An CH, Hollerbach JM. Estimation of inertial parameters of manipulator loads and links. Int J Robot Res 1986;5:101–19.
[20] Calafiore G, Indri M, Bona B. Robot dynamic calibration: optimal excitation trajectories and experimental parameter estimation. J Robot Syst 2001;18:55–68.
[21] Presse C, Gautier M. New criteria of exciting trajectories for robot identification. In: International conference on robotics and automation, 1993, p. 907–12.
[22] Swevers J, Naumer B, Pieters S, Biber E, Verdonck W, Schutter JD. An experimental robot load identification method for industrial application. Int J Robot Res, 2002;21:701–12.
[23] Cleveland WS. Robust locally weighted regression and smoothing scatterplots. J Am Stat Assoc 1979;74:829–36.
[24] Spong MW. On the robust control of robot manipulators. IEEE Trans Autom Control 1992;37:1782–6.
[25] Jaritz A, Spong MW. An experimental comparison of robust control algorithms on a direct drive manipulator. IEEE Trans Control Syst Technol 1996;4:627–40.
[26] Khalil W, Dombre E. Modeling, identification and control of robots, 3rd ed. New York: Taylor and Francis Group; 2002.
[27] Khalil W, Gautier M, Lemoine P. Identification of the payload inertial parameters of industrial manipulators. In: International conference on robotics and automation, 2007, p. 4943–8.
[28] Mayeda H, Yoshida K, Osuka K. Base parameters of manipulator dynamic models. IEEE Trans Robot Autom 1990;6:312–21.
[29] Gautier M. Numerical calculation of the base inertial parameters of robots. J Robot Syst 1991;8:485–506.
[30] Gautier M, Briot S. Dynamic parameter identification of a 6 dof industrial robot using power model. In: International conference on robotics and automation, 2013, p. 2914–20.
[31] Gautier M, Janot A, Vandanjon P. A new method for the dynamic identification of robots from only torque data. In: International conference on robotics and automation, 2008, p. 2122–7.
[32] Swevers J, Verdonck W, Schutter JD. Dynamic model identification for industrial robots. IEEE Control Syst Mag 2007;5:58–71.
[33] Garling DJH. Inequalities: a journey into linear analysis. Cambridge University Press, Cambridge, UK; 2007.
[34] ⟨http://www.staubli.com⟩, 2009.